

# SPICEE: An Extension of SPICE for Sparse Endmember Estimation in Hyperspectral Imagery

Seniha Esen Yuksel, *Member, IEEE*, Sefa Kucuk, *Student Member, IEEE*, and Paul D. Gader, *Fellow, IEEE*

**Abstract**—An extension to the sparsity promoting iterated constrained endmember (SPICE) algorithm, named as SPICEE, has been presented. In ICE and SPICE, endmembers are estimated using a pseudoinverse method, which may generate endmembers that are not physically possible when representing normalized reflectance spectra. Although this problem can be alleviated by increasing the regularization, too much regularization leads to finding erroneous endmembers. To solve these problems, in this letter, a quadratic optimization solution is proposed that constrains the endmembers to have values between zero and one. The results on three data sets indicate that when regularization is large enough, SPICE and SPICEE generate similar answers; and when regularization is small to none, SPICEE stays more robust. In doing so, besides generating realistic endmembers, SPICEE helps in decreasing the effort necessary for fine-tuning the regularization parameter.

**Index Terms**—Endmember, quadratic optimization (QP), sparsity promoting iterated constrained endmember (SPICE).

## I. INTRODUCTION

IN HYPERSPECTRAL imaging, one of the problems of considerable interest is to automatically estimate the endmembers and the number of endmembers in a given scene. Iterated constrained endmembers (ICE) [1] and sparsity promoting ICE (SPICE) [2] as well as other studies [3]–[7] require to compute a pseudoinverse for finding the endmembers that do not put any constraints on the endmembers. In this letter, an extension to the SPICE algorithm, named SPICEE, is presented which solves for the endmembers using quadratic optimization (QP) and constrains the values to be in  $[0, 1]$ , thereby producing more realistic endmembers.

In Section II, a review of the SPICE algorithm is provided. In Section III, SPICEE is derived. In Section IV, experimental results on simulated and real hyperspectral data sets are presented. Finally, the concluding remarks are given in Section V.

Manuscript received April 29, 2016; revised August 13, 2016 and September 23, 2016; accepted October 9, 2016. Date of publication November 1, 2016; date of current version December 7, 2016. This work was supported by the Scientific and Technological Research Council of Turkey (TUBITAK) under Project 115E318.

S. E. Yuksel and S. Kucuk are with the Department of Electrical and Electronics Engineering, Hacettepe University, 06800 Ankara, Turkey (e-mail: eyuksel@ee.hacettepe.edu.tr; skucuk@ee.hacettepe.edu.tr).

P. D. Gader is with the Department of Computer and Information Science and Engineering, University of Florida, Gainesville, FL 32611 USA (e-mail: pgader@cise.ufl.edu).

Color versions of one or more of the figures in this paper are available online at <http://ieeexplore.ieee.org>.

Digital Object Identifier 10.1109/LGRS.2016.2617316

## II. REVIEW OF ICE AND SPICE

Let  $\mathbf{X}$  denote the  $d \times N$  matrix of pixels in a hyperspectral image where  $N$  is the number of pixels and  $d$  is the number of hyperspectral bands. Each column of this matrix,  $\mathbf{X}_i$  is the  $d \times 1$  vector representing the  $i$ th pixel in the image. Also, the rows of  $\mathbf{X}$  are used to form the  $N \times 1$  vector  $\mathbf{x}_j$ ,  $j = 1, \dots, d$  where  $\mathbf{x}_j$  denotes the  $N$  observations in the  $j$ th spectral band. In addition, let  $M$  be the number of endmembers in a scene, and  $e_{kj}$  be the value of the  $k$ th endmember in the  $j$ th spectral band. These endmembers can be represented by the  $d \times M$  endmember matrix  $\mathbf{E}$ , where a column of this matrix  $\mathbf{E}_k$  is the  $d \times 1$  vector representing the  $k$ th endmember. Therefore,  $\mathbf{E}_k^T = (e_{k1}, \dots, e_{kd})$ . Also, the rows of  $\mathbf{E}$  are used to form the vector  $\mathbf{e}_j^T = (e_{1j}, \dots, e_{Mj})$ , where  $\mathbf{e}_j$  is the  $M \times 1$  vector of endmember values in the  $j$ th spectral band.

Both ICE and its sparse extension, SPICE, follow the linear mixing model

$$\mathbf{X}_i = \sum_{k=1}^M p_{ik} \mathbf{E}_k + \epsilon_i \quad i = 1, \dots, N \quad (1)$$

where  $\epsilon_i$  is an error term and  $p_{ik}$  is the proportion of endmember  $k$  in pixel  $i$ . The proportions satisfy the constraints

$$\sum_{k=1}^M p_{ik} = 1, \quad p_{ik} \geq 0; \quad k = 1, \dots, M. \quad (2)$$

In addition, in the rest of this letter,  $\mathbf{P}$  will denote the  $N \times M$  matrix of proportions of the endmembers for all the pixels.

SPICE algorithm estimates the endmembers and proportion values by minimizing the objective function  $RSS_{\text{reg}}^*$

$$RSS_{\text{reg}}^* = (1 - \mu) \frac{RSS}{N} + \mu V + SPT \quad (3)$$

subject to the constraints in (2). Here,  $RSS$  is the residual sum of squares,  $V$  is a regularization term,  $SPT$  is the sparsity promoting term, and  $\mu$  is a regularization parameter in  $(0, 1)$  that provides a tradeoff between the  $RSS$  and  $V$  as defined in [1]. The  $RSS$  term in (3) provides the least square minimization of (1), and is computed as

$$RSS = \sum_{j=1}^d (\mathbf{x}_j - \mathbf{P}\mathbf{e}_j)^T (\mathbf{x}_j - \mathbf{P}\mathbf{e}_j). \quad (4)$$

The *SPT* term in (3) is the sparsity-promoting term

$$\text{SPT} = \sum_{k=1}^M \gamma_k \sum_{i=1}^N p_{ik} \quad (5)$$

$$\gamma_k = \frac{\Gamma}{\sum_{i=1}^N p_{ik}} \quad (6)$$

and  $\Gamma$  is a constant that determines the degree to which the proportion values are driven to zero [2].

With all these terms defined, (3) needs to be minimized over both the proportions for each pixel, and for the  $M$  endmembers. ICE and SPICE both do this iteratively: given the endmember estimates, they estimate the proportion matrix  $\mathbf{P}$  and given the proportion estimates, they estimate the endmembers. To find the endmembers, both ICE and SPICE solve (3) by a pseudoinverse solution [1].

### III. SPICEE

SPICEE also finds the endmembers and proportions iteratively, with the major difference being in finding endmembers.

#### A. Finding the Proportions

The  $V$  term in (3) does not depend on the proportions. The remaining terms can be solved by a least squares minimization of each of the  $N$  terms subject to the linear constraints in (2). This is accomplished by QP in ICE, SPICE, and SPICEE. Practically, solving by QP means that the optimization function

$$J(E, P; x) = (1 - \mu) \frac{\text{RSS}}{N} + \text{SPT}$$

is rearranged in the form of  $p'Ap + p'b$ , and these  $A$  and  $b$  values are fed into standard optimization libraries.

#### B. Finding the Endmembers

In finding the endmembers with the pseudoinverse, both ICE and SPICE can produce endmembers that are below zero or larger than one. However, reflectance is generally between 0 and 1; except for the cases of highly reflective man-made materials. In scenes where such materials do not exist, we would like to prevent unrealistic solutions. Therefore, we solve the endmembers using QP, and introduce the following constraint.

Let  $\mathbf{e}_j$  be all the endmembers of the  $j$ th spectral band such that  $\mathbf{e}_j^T = (e_{1j}, \dots, e_{kj}, \dots, e_{Mj})$  where  $j = 1, \dots, d$ . Each of these values should satisfy  $0 \leq e_{kj} \leq 1$ .

With these constraints, the minimization turns into a QP problem as opposed to the pseudoinverse. First, the SPT term does not depend on any endmembers. Therefore, the remaining terms in (3) can be written as

$$\text{RSS}_{\text{new}} = (1 - \mu) \frac{\text{RSS}}{N} + \mu V. \quad (7)$$

The terms in  $\text{RSS}_{\text{new}}$  can be rearranged as shown in (8). Note that the terms independent of  $\mathbf{e}_j$  were dropped going from the

first line to the second line

$$\begin{aligned} \text{RSS}_{\text{reg}} &= \frac{(1 - \mu)}{N} \sum_{j=1}^d (\mathbf{x}_j - \mathbf{P}\mathbf{e}_j)^T (\mathbf{x}_j - \mathbf{P}\mathbf{e}_j) \\ &\quad + \mu \frac{1}{M(M-1)} \sum_{j=1}^d \mathbf{e}_j^T (M\mathbf{I}_M - \mathbf{1}\mathbf{1}^T) \mathbf{e}_j \\ &\simeq \sum_{j=1}^d \left\{ \frac{(1 - \mu)}{N} \mathbf{e}_j^T (\mathbf{P}^T \mathbf{P}) \mathbf{e}_j + \frac{(1 - \mu)}{N} (-2) \mathbf{e}_j^T \mathbf{P}^T \mathbf{x}_j \right. \\ &\quad \left. + \frac{\mu}{M(M-1)} \mathbf{e}_j^T (M\mathbf{I}_M - \mathbf{1}\mathbf{1}^T) \mathbf{e}_j \right\} \\ &= \frac{(1 - \mu)}{N} \sum_{j=1}^d \mathbf{e}_j^T H \mathbf{e}_j + \mathbf{e}_j^T f. \end{aligned} \quad (8)$$

In (8), the terms forming the optimization function are as follows:

$$H = \mathbf{P}^T \mathbf{P} + \lambda \left( \mathbf{I}_M - \frac{\mathbf{1}\mathbf{1}^T}{M} \right) \quad (9)$$

$$f = -2\mathbf{P}^T \mathbf{x}_j \quad (10)$$

$$\lambda = \frac{N\mu}{(M-1)(1-\mu)}. \quad (11)$$

Note that this is the same form as in the proportion estimation, and the standard QP code used in proportion estimation can be used for endmember estimation. Finally, the optimization is performed for each band, and the boundary constraints for the upper bound  $ub$  and lower bound  $lb$  are given as  $lb = \mathbf{0}$  and  $ub = \mathbf{1}$  where  $\mathbf{0}$  is the  $M \times 1$  zero vector and  $\mathbf{1}$  is the  $M \times 1$  vector of ones. This constricts the endmembers to be between  $[0, 1]$ .

### IV. EXPERIMENTAL RESULTS

In this section, we provide the results on three data sets. The first is a toy example with three endmembers and two bands. The second is a simulated data obtained from the signatures in the Advanced Spaceborne Thermal Emission and Reflection Radiometer (ASTER) library with 5 endmembers and 258 bands. The third data set is the real data of Pavia University with 103 bands and 9 different classes.

#### A. Toy Example

Three endmembers were selected as the corners of a triangle with coordinates  $([0, 0]; [0, 1]; [1, 0])$ . In addition, random numbers were generated and were normalized to sum to 1 to make the proportions. Then data were generated from the proportions and endmembers by following the linear mixing model as in (1). In addition, to examine the behavior of the algorithms on noisy data, three noisy endmember sets were generated. Three signal-to-noise ratio (SNR) levels were obtained as 79.54, 63.58, and 45.02 dB, which were varied by changing the variance of Gaussian. The noise levels were generated from Gaussian distribution with zero mean and variances 0.001, 0.01, and 0.1, respectively. SPICE and SPICEE are compared with decreasing levels of SNR using the earth movers distance (EMD) [9] with squared Euclidean distance

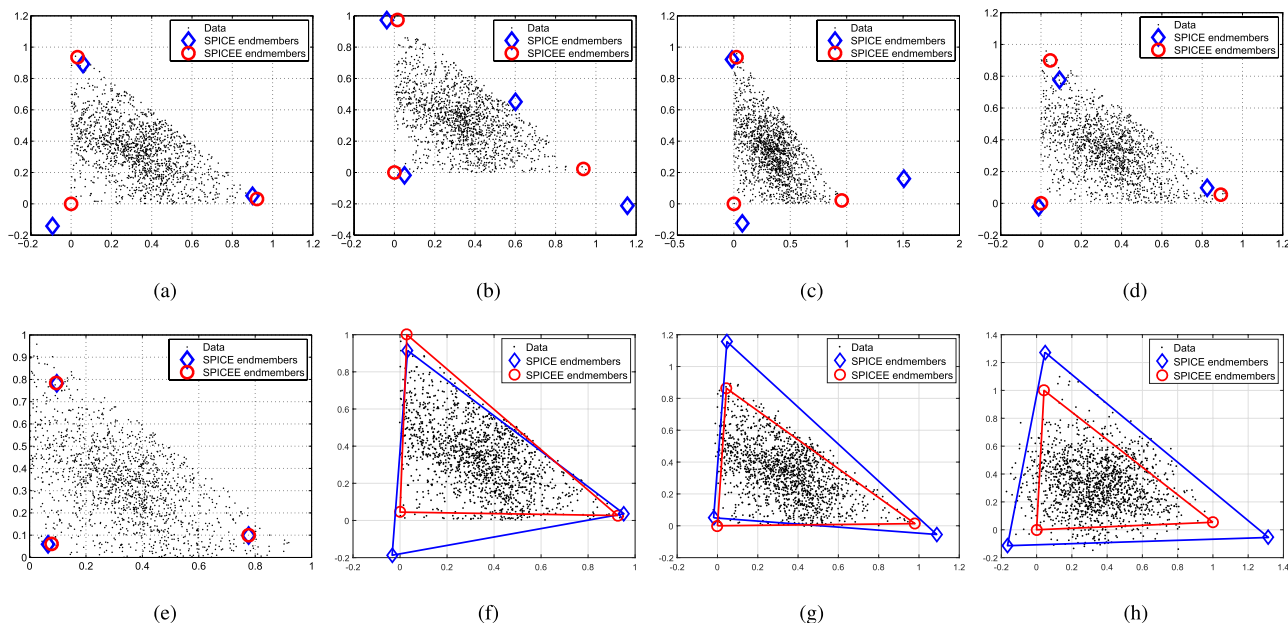


Fig. 1. Comparison of SPICE and SPICEE on toy data. The sparsity term  $\gamma = 1$  in all the experiments. (a) Three endmembers,  $\mu = 0$ . Both SPICE and SPICEE were initialized with three endmembers.  $\mu = 0$  indicating the regularization term was ignored and the biggest possible box was found. In such a case, SPICE finds endmembers that are smaller than 0, which is not physically possible. (b) Twenty endmembers,  $\mu = 0$ . Both SPICE and SPICEE were initialized with 20 endmembers, and the regularization tradeoff  $\mu = 0$ . For the same set of parameters, SPICE found four endmembers and two of them had negative coordinates, whereas SPICEE was better at staying in the  $[0, 1]$  range and found only three endmembers. (c) Twenty endmembers,  $\mu = 0.0001$ . When the regularization tradeoff was increased to  $\mu = 0.0001$ , the box of SPICE shrunk, but the results were not much better and negative endmembers could still be observed. (d) Twenty endmembers,  $\mu = 0.001$ . Similarly, at  $\mu = 0.001$ , the bottom left endmember was found to be  $[-0.0116, -0.0237]$  by SPICE as opposed to  $[0, 0]$  by SPICEE. (e) Twenty endmembers,  $\mu = 0.01$ . Only when  $\mu = 0.01$ , SPICEE and SPICE resulted in the same endmembers that were in the  $[0, 1]$  range. However, this has been at the expense of not finding the real endmembers [8]. The algorithms were initialized with 20 endmembers and  $\mu = 0$  for noisy data sets. EMD values were computed between the estimated endmembers and proportions and the real values used to generate the data sets. (f) SNR = 79.54 dB. EMD\_SPICE = 127.09. EMD\_SPICEE = 64.83. Both the algorithms found three endmembers but SPICE found a negative endmember. (g) SNR = 63.58 dB. EMD\_SPICE = 136.09. EMD\_SPICEE = 87.13. SPICE found the endmembers out of  $[0, 1]$  range and the EMD values increased. (h) SNR = 45.02 dB. EMD\_SPICE = 532.04. EMD\_SPICEE = 266.98. For SNR = 45.02 dB level when the endmember data set become more noisy, SPICE and SPICEE found the correct number of endmembers but obtained large estimated EMD values. In addition, SPICEE stayed in the  $[0, 1]$  range.

as the ground distance. For the same set of parameters, SPICE and SPICEE were compared for nonnoisy data in Fig. 1(a)–(e) and for noisy data in Fig. 1(f)–(h).

It can be seen from Fig. 1 that SPICE can lead to negative values or values larger than 1. To prevent such cases,  $\mu$  needs to be increased, however, a smaller convex hull may result in missing the real endmember values. On the other hand, SPICEE always estimates the endmembers to be in the  $[0, 1]$  range, and can benefit from a regularization term if needed. Beyond a value for  $\mu$ , both SPICE and SPICEE result in similar estimates of the endmembers. When we compared EMD values, SPICE resulted in larger EMD distances than SPICEE for all noisy data sets. In addition, the EMD distances increased with increasing noise levels for both the algorithms. When the noise forces the data to go beyond the  $[0, 1]$  range, SPICE tends to find the convex hull of the noisy data and estimates endmembers out of the  $[0, 1]$  range; SPICEE on the other hand stays more robust and stays in the  $[0, 1]$  range. However, if there are highly specular materials with reflectance values out of the  $[0, 1]$  range, SPICEE would also pull them to the  $[0, 1]$  range.

### B. Simulated Hyperspectral Data From the ASTER Library

The ASTER spectral library [10] was used to generate simulated hyperspectral data. Five different endmembers, namely,

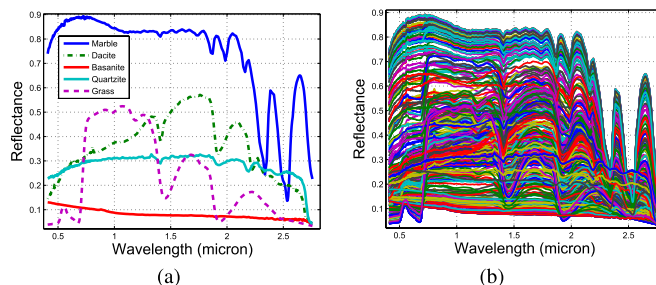


Fig. 2. Simulated data. (a) Five endmembers from ASTER. (b) Simulated data were generated using the five endmembers and the proportion values generated from the Dirichlet distribution.

the marble, dacite, basanite, quartzite, and grass were selected from the library as shown in Fig. 2(a). The proportions of the endmembers were generated using Dirichlet distribution and simulated hyperspectral data was generated using the linear mixing model. The simulated hyperspectral data are shown in Fig. 2(b).

Both SPICE and SPICEE were applied to simulated data to retrieve the endmembers and identify the correct number of endmembers. The estimated endmembers were compared with ASTER library spectra. The errors between the library spectra and the estimated endmembers were calculated using spectral angle mapper (SAM) and Euclidean distances (EDs).

TABLE I

COMPARISON OF ENDMEMBERS FOUND BY THE ALGORITHMS IN 100 EXPERIMENTS WITH THE SAME INITIALIZATION. THE FIRST ROW SHOWS HOW MANY TIMES THE ALGORITHMS FOUND THE NUMBER OF ENDMEMBERS CORRECTLY. THE SECOND ROW SHOWS HOW MANY TIMES THE ALGORITHMS FOUND THE ENDMEMBERS TO BE SMALLER THAN 0 AND THE THIRD ROW SHOWS HOW MANY TIMES THE ENDMEMBERS WERE FOUND TO BE BIGGER THAN 1. THE THIRD AND FOURTH ROWS SHOW THE AVERAGE ERROR BETWEEN THE ASTER ENDMEMBERS AND THE ESTIMATED ENDMEMBERS AND ITS STANDARD DEVIATION. THE SIXTH ROW SHOWS EMD VALUES BETWEEN UNMIXING RESULTS AND THE TRUE VALUES. THE LAST ROW SHOWS THE COMPUTATIONAL TIME OF ALGORITHMS

	SPICE			SPICEE		
	$\mu = 0$	$\mu = 0.0001$	$\mu = 0.01$	$\mu = 0$	$\mu = 0.0001$	$\mu = 0.01$
Is the number of endmember = 5?	97/100	99/100	100/100	99/100	100/100	100/100
The minimum value < 0	27/100	27/100	0/100	0/100	0/100	0/100
The maximum value > 1	3/100	5/100	0/100	0/100	0/100	0/100
The average SAM error	$0.040 \pm 0.033$	$0.037 \pm 0.032$	$0.018 \pm 0.002$	$0.036 \pm 0.031$	$0.022 \pm 0.003$	$0.018 \pm 0.002$
The average ED error	$0.269 \pm 0.243$	$0.267 \pm 0.100$	$0.281 \pm 0.077$	$0.267 \pm 0.241$	$0.261 \pm 0.218$	$0.272 \pm 0.064$
The average EMD values	$669.78 \pm 870.49$	$714.52 \pm 582.71$	$423.24 \pm 89.05$	$643.47 \pm 581.37$	$401.44 \pm 132.32$	$423.96 \pm 85.51$
The average elapse time (Sec.)	0.98	1.03	1.04	1.25	1.25	1.28

In addition, EMD values between the unmixing results and the true values were computed. SPICEE was compared with SPICE for the same set of parameters (the initial number of endmembers was set to 10,  $\Gamma = 1$ , pruning threshold = 0.0007 and regularization term was set to  $\mu = 0$ ,  $\mu = 0.0001$ ,  $\mu = 0.01$ ; respectively). The algorithms were run 100 times on simulated data and the average error between the library spectra and estimated endmembers are reported in Table I. The average SAM and ED were computed for the cases when the algorithms found the correct number of endmembers as 5. EMD eliminated this problem because EMD could compare unmixing results with different number of endmembers. The first row in Table I shows that SPICEE has found the correct number of endmembers slightly more than SPICE in all the cases. In rows 2 and 3, SPICE found the endmembers out of the  $[0, 1]$  range in many cases, and the regularization term had to increase in order for SPICE to find endmembers in the desired range. However, SPICEE always stayed in the  $[0, 1]$  range, irrespective of the changes in regularization, and obtained very similar results to SPICE when the regularization term was larger. In addition, when we compared the average errors, SPICEE found the endmembers with less error and SPICEE had smaller EMD values except for  $\mu = 0.01$ . Even then, the EMD values are pretty close and looking at the variances, the difference is not statistically significant. Concerning the elapse time of algorithms, SPICE is faster than SPICEE as the former uses the pseudoinverse and SPICEE solves the endmembers using QP. The experiments were run on a personal computer with Windows 8.1 Intel Core 2.4 GHz and 16 GB RAM. Of the 100 experiments, one sample result initialized with  $\mu = 0$  and 10 endmembers is given in Fig. 3. Here, SPICE found 6 endmembers as opposed to 5, and some endmembers were negative and some bigger than 1. On the other hand, SPICEE found five endmembers correctly in the  $[0, 1]$  range with less error.

In our experiments on the ASTER library, when our assumption did not hold, and the true endmembers were out-of-the  $[0, 1]$  range for materials with large specular glint as in Fig. 4, SPICEE was seen to truncate these endmembers to  $[0, 1]$ , was successful in finding the other endmembers that stayed in the range, but had problems finding the true proportions.

We also compared SPICEE with minimum volume simplex analysis (MVSA) [11] based on EMD distances.

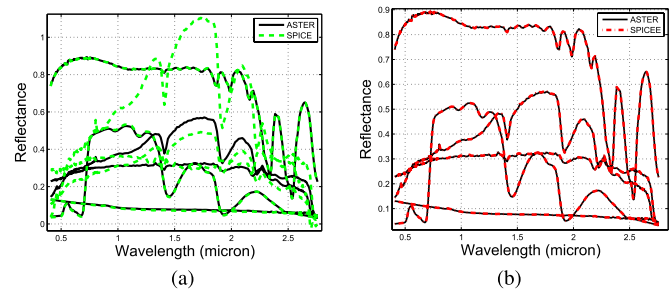


Fig. 3. Comparison of endmembers that were estimated by SPICE and SPICEE. (a) Library endmembers versus estimated endmembers by SPICE. SPICE found six endmembers as opposed to 5. In addition, the minimum and maximum of two endmembers were found to be  $[-0.007, 1.277]$ . (b) Library endmembers versus estimated endmembers by SPICEE. SPICEE found five endmembers in the  $[0, 1]$  range. Also, SPICEE was able to better follow the library spectra.

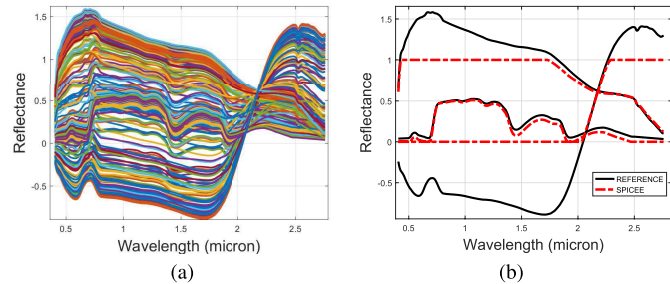


Fig. 4. (a) Simulated data. Simulated data were generated using three endmembers of which two are out-of-the  $[0, 1]$  range. (b) Reference versus SPICEE. Estimated endmembers by SPICEE.

MVSA performed better than SPICEE if the endmembers were in the range and the numbers of endmembers were known. On the other hand, SPICEE estimates the number of endmembers and does not result in negative values as opposed to MVSA.

### C. Real Data From ROSIS Pavia University Data Set

The algorithms were also tested on the ROSIS Pavia University data set [12]. The image has 103 spectral bands between  $(0.43\text{--}0.86) \mu\text{m}$  and a spatial resolution of 1.3 m.

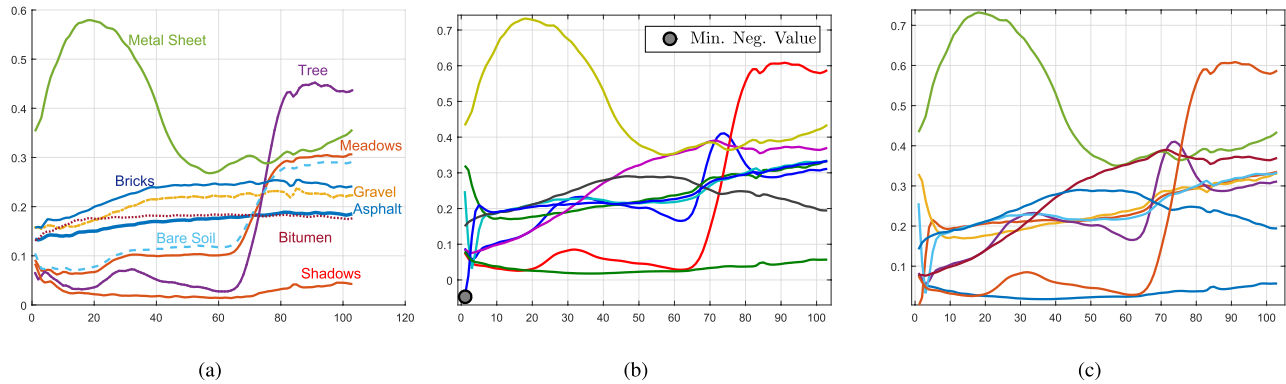


Fig. 5. (a) Ground truth endmembers. Endmember spectra of nine classes. (b) Estimated endmembers by SPICE. SPICE found negative endmember values. (c) Estimated endmembers by SPICEE. SPICEE stayed in the  $[0, 1]$  range.

TABLE II  
COMPARISON OF SPICE AND SPICEE ON THE PAVIA UNIVERSITY  
DATA SET ON 100 RUNS WITH THE SAME INITIALIZATIONS

	SPICE	SPICEE
The number of endmember	9 - 11	9 - 11
The minimum value $< 0$	94/100	0/100
The maximum value $> 1$	0/100	0/100
The average SAM error	$0.144 \pm 0.093$	$0.148 \pm 0.092$
The average ED error	$0.664 \pm 0.308$	$0.674 \pm 0.306$

Both the algorithms were compared for the same set of parameters (the initial number of endmembers was set to 20,  $\Gamma = 1$ , pruning threshold = 0.0007 and  $\mu = 0.01$ ). They were tested 100 times and the errors between the reference and the estimated spectra were calculated. To compute the errors, the endmember spectra were extracted from the classes of the ground truth by averaging. The manually selected area's spectra are shown in Fig. 5(a). It can be seen that three endmembers: trees, shadow, and metal sheets have distinguishable spectra. The other six endmembers have very similar patterns and therefore it is difficult to separate them from the unmixing data set. The reference endmember spectra were compared with the estimated results of the algorithms as indicated in Table II. Both the algorithms found a varying number of endmembers between 9 and 11. SPICE found the negative endmember values in almost all the experiments despite a large regularization term ( $\mu = 0.01$ ). However, SPICEE stayed in the  $[0, 1]$  range in all the experiments. When we compared the average SAM and ED distance errors, the results were almost the same. These average errors were computed only for the cases when the algorithms found the correct number of endmembers. Fig. 5 shows the endmember spectra found in one experiment. It can be seen that both SPICE and SPICEE pruned the unnecessary endmembers and found nine endmembers. The algorithms estimated the endmembers successfully, especially for the trees, shadows, and metal sheets classes.

## V. CONCLUSION

SPICE is a powerful algorithm that allows estimating the endmembers as well as the number of endmembers. However, as we show in this letter, without proper parameter tuning, small regularization terms, it is possible to get endmembers

that are out of the  $[0, 1]$  range. On the other hand, setting the regularization term to a higher value may result in incorrect endmember estimation. To alleviate these problems, we have introduced SPICEE that solves the endmember estimation through QP as opposed to taking the pseudoinverse. Our comparative results on three data sets indicate that SPICEE is more robust to parameter tuning if the regularization parameter is chosen to be small; and gives results similar to SPICE when they are highly regularized.

## REFERENCES

- [1] M. Berman, H. Kiveri, R. Lagerstrom, A. Ernst, R. Dunne, and J. F. Huntington, "ICE: A statistical approach to identifying endmembers in hyperspectral images," *IEEE Trans. Geosci. Remote Sens.*, vol. 42, no. 10, pp. 2085–2095, Oct. 2004.
- [2] A. Zare and P. Gader, "Sparsity promoting iterated constrained end-member detection in hyperspectral imagery," *IEEE Geosci. Remote Sens. Lett.*, vol. 4, no. 3, pp. 446–450, Jul. 2007.
- [3] A. Zare and P. Gader, "Hyperspectral band selection and endmember detection using sparsity promoting priors," *IEEE Geosci. Remote Sens. Lett.*, vol. 5, no. 2, pp. 256–260, Apr. 2008.
- [4] A. Zare *et al.*, "Sub-pixel target spectra estimation and detection using functions of multiple instances," in *Proc. 3rd Workshop WHISPERS*, Jun. 2011, pp. 1–4.
- [5] C. R. Ratto, K. D. Morton, L. M. Collins, and P. A. Torriero, "A comparison of principal components and endmember-based contextual learning for hyperspectral anomaly classification," in *Proc. 3rd Workshop WHISPERS*, Jun. 2011, pp. 1–4.
- [6] Y. Rezaei, M. R. Mobasheri, M. J. V. Zoej, and M. E. Schaepman, "Endmember extraction using a combination of orthogonal projection and genetic algorithm," *IEEE Geosci. Remote Sens. Lett.*, vol. 9, no. 2, pp. 161–165, Mar. 2012.
- [7] A. Zare and P. G. Senior, "Sparsity promoting iterated constrained endmember detection with integrated band selection," in *Proc. IEEE IGARSS*, Jul. 2007, pp. 4045–4048.
- [8] S. E. Yuksel, "Endmember detection using enhanced constrained optimization in hyperspectral imaging," in *Proc. 22nd Signal Process. Commun. Appl. Conf. (SIU)*, Apr. 2014, pp. 1023–1026.
- [9] A. Zare and D. T. Anderson, "Earth movers distance-based simultaneous comparison of hyperspectral endmembers and proportions," *IEEE J. Sel. Topics Appl. Earth Observ. Remote Sens.*, vol. 7, no. 6, pp. 1910–1921, Jun. 2014.
- [10] A. M. Baldridge, S. J. Hook, C. I. Grove, and G. Rivera, "The ASTER spectral library version 2.0," *Remote Sens. Environ.*, vol. 113, no. 4, pp. 711–715, Apr. 2009.
- [11] J. Li, A. Agathos, D. Zaharie, J. M. Bioucas-Dias, A. Plaza, and X. Li, "Minimum volume simplex analysis: A fast algorithm for linear hyperspectral unmixing," *IEEE Trans. Geosci. Remote Sens.*, vol. 53, no. 9, pp. 5067–5082, Sep. 2015.
- [12] *Hyperspectral Remote Sensing Scenes*. accessed on Jun. 23, 2014. [Online]. Available: [http://www.ehu.eus/ccwintco/index.php?title=Hyperspectral\\_Remote\\_Sensing\\_Scenes#Pavia\\_University\\_scene](http://www.ehu.eus/ccwintco/index.php?title=Hyperspectral_Remote_Sensing_Scenes#Pavia_University_scene)